Hindawi
Advances in Meteorology
Volume 2018, Article ID 4714173, 14 pages
https://doi.org/10.1155/2018/4714173

Research Article

Evaluation and Correction of GPM IMERG Precipitation Products over the Capital Circle in Northeast China at Multiple Spatiotemporal Scales

Wei Sun,[1,2,3] Yonghua Sun,[1,2,3] Xiaojuan Li,[1,2,3] Tao Wang,[1,2,3] Yanbing Wang,[1,2,3] Qi Qiu,[1,2,3] and Zhitian Deng[1,2,3]

[1]*College of Resource Environment and Tourism, Capital Normal University, Beijing 100048, China*
[2]*College of Geospatial Information Science and Technology, Capital Normal University, Beijing 100048, China*
[3]*Beijing Laboratory of Water Resource Security, Capital Normal University, Beijing 100048, China*

Correspondence should be addressed to Yonghua Sun; sunyonghua@cnu.edu.cn and Xiaojuan Li; lixiaojuan@cnu.edu.cn

Received 11 July 2018; Revised 6 October 2018; Accepted 6 November 2018; Published 13 December 2018

Academic Editor: Federico Porcù

Accurate remote-sensed precipitation data are crucial to the effective monitoring and analysis of floods and climate change. The Global Precipitation Measurement (GPM) satellite product offers new options for the global study of precipitation. This paper evaluates the applicability of GPM IMERG products at different time resolutions in comparison to ground-measured data. Based on precipitation data from 107 meteorological stations in the Beijing-Tianjin-Hebei region, GPM products were analysed at three timescales: half-hourly (GPM-HH), daily (GPM-D), and monthly (GPM-M). We use a cumulative distribution function (CDF) model to correct GPM-D and GPM-M products to analyse temporal and spatial distributions of precipitation. We came to the following conclusions: (1) The GPM-M product is strongly correlated with ground station data. Based on five evaluation indexes, NRMSE (Normalized Root Mean Square Error), NSE (Nash-Sutcliffe), FAR (False Alarm Ratio), UR (Underreporting Rate), and CSI (Critical Success Index), the monthly GPM products showed the best performance, better than GPM-HH products and GPM-D products. (2) The performance of GPM products in summer and autumn was better than in winter and spring. However, the GPM satellite's precision in undulating terrain was poor, which could easily lead to serious errors. (3) CDF models were successfully used to modify GPM-D and GPM-M products and improve their accuracy. (4) The range of 0–100 mm precipitation could be corrected best, but the GPM-M products were underestimated. Corrected GPM-M data in the range >100 mm were overestimated. According to this analysis, the GPM IMERG Final Run products at daily and monthly timescales have good detection ability and can provide data support for long-time series analyses in the Beijing-Tianjin-Hebei region.

1. Introduction

Precipitation is an important part of the water cycle of terrestrial ecosystems [1] and has a profound impact on atmospheric and hydrological processes. Precipitation is one of the most important hydrological meteorological variables [2] as it provides the underlying data of most studies on hydrology, climatology, and ecology [1]. At present, the meteorological observations of the national basic meteorological observing stations and the surface precipitation radar are the main observation methods for rainfall. However, while the rainfall data of gauges are highly accurate, only the precipitation data of the corresponding point can be obtained [3]. Therefore, it is hard to fully reflect the spatial distribution and changes in rainfall intensity [2]. Also, there is a lack of data on polar, marine, and remote mountainous areas. Although ground-based rain radars can indirectly obtain precipitation information with high temporal and spatial resolution, their accuracy is affected by the spatial structure of the ground and their observation range is limited [3].

In recent decades, the development of remote sensing and geographic information systems and generation of

corresponding remote-sensing product data have provided entirely new methods and means for precipitation observation [4]. The successful launch of the Tropical Rainfall Measuring Mission (TRMM) has created a new era of global satellite rainfall monitoring [2] TRMM carries the first space-borne precipitation radar (PR), which provides 3D precipitation echo information. The Global Precipitation Measurement (GPM), a new generation of satellite precipitation products, is a follow-up to the TRMM. Comprehensive assessments of the TRMM satellite in China have been carried out, including accuracy evaluation of space scale and drought and waterlogging events, based on the different timescales of the TRMM satellites [5–10]. As the new generation of precipitation observing satellites, GPM provides more options for studying precipitation, and currently, scholars from different regions of the world have conducted preliminary assessments of GPM IMERG and TRMM products. Some assessments of the GPM (IMERG) have been conducted in Iran [11, 12], Korea [13], Japan [13], the Blue Nile Basin [14], Southern Canada [15], India [16], Singapore [17], Austria [18], the Main Bolivian Watersheds [19], and Peru [20]. GPM-3IMERGHH is more accurate than TRMM 3B42 V7 in describing the spatial distribution of precipitation [13, 16]. Chiaravalloti [21] assessed GPM and SM2RAIN-ASCAT rainfall products over complex terrain in southern Italy and found that MERG has good performance at the time resolution greater than 6h. However, there are still several uncertainties in different regions, time periods, topography, and precipitation patterns [17]. In China, many scholars have studied the precision of the GPM [22–28, 36]. Comparing GPM products with the TRMM (3B42V7) product, it was found that GPM performed better than TRMM in relatively dry climates. On the monthly scale, the accuracy of GPM in winter precipitation in mainland China is obviously better than that of TRMM because GPM improves the observational ability of weak precipitation and solid precipitation [29, 30]. At the same time, GPM can detect the changes in precipitation day by day [22]. In extreme precipitation events, all the GPM IMERG products are superior to the TRMM series of satellites [17]. In different elevation zones of the Tianshan Mountains, the GPM showed lower error and a higher correlation coefficient with the observation stations [25].

Remote-sensing data include regional and seasonal systematic deviations and random errors. These deviations can be corrected by calibrating the data with rainfall data measured by on-ground weather stations [31, 32]. Many scholars at home and abroad have done a lot of work on the error correction of satellite precipitation products. Common methods are interpolation method, physical model method, and statistical model method. AghaKouchak et al. (2009) corrected the uncertainty of precipitation by establishing a two-parameter stochastic model and used the maximum likelihood to estimate the random error and the multiplication error to correct the TRMM data [33]. Cheema and Bastiaanssen (2012) used the regression analysis (RA) and geographic difference analysis (GDA) to locally correct the TRMM3B43 precipitation data and found that the GDA calibration method performed best in the mountainous area [34]. However, research on Global Precipitation Measurement (GPM) products mostly focuses on verification of the accuracy of data from different regions; however, research on GPM product data correction is scarce. Guo et al. (2016) conducted accuracy verification on the GPM data before and after the calibration of the Global Precipitation Climate Centre (GPCC) monthly data. It was found that the correlation coefficient of the calibrated GPM data products in the national and regional areas was significantly improved and the relative error was reduced [35]. Jin et al. (2018) used the MERGE error correction method to reduce the precipitation error in high-altitude areas effectively [36]. According to the research into TRMM data correction, cumulative distribution function (CDF) models can be fitted to precipitation distribution data by using the gamma distribution of two parameters [32, 37]. For cumulative precipitation data, the CDF model uses a cumulative distribution function based on multiyear precipitation, which is suitable for spatial and temporal data correction [38–40].

At present, research evaluating the applicability of the GPM products and correction in Beijing, Tianjin, and Hebei Province is relatively scarce. Precipitation is one of the important sources of water resources in Beijing, Tianjin, and Hebei [41]. Rainstorm events can cause serious economic losses in the area, adversely affecting urban operations (roads, transport, etc.) [42]. Therefore, a focus on precipitation events in the Beijing–Tianjin–Hebei region is important. In this paper, our purposes are as follows: (1) to evaluate the performance of the post-real-time GPM IMERG Final Run product at three temporal resolutions (i.e., half-hourly, daily, and monthly) over the Beijing–Tianjin–Hebei region of China; (2) to analyse the applicability of GPM-M products at different rainfall intensities and regions; (3) to correct the GPM-M products and the GPM-D products by using CDF model to improve accuracy; and (4) to analyse the temporal and spatial distribution characteristics of precipitation based on modified GPM-M products. This paper is organized as follows: Section 2 introduces the study area and the different data sets used in this study; Section 3 describes the methodologies used for evaluation and correction; Section 4 presents the results and discussion; and finally, Section 5 provides concluding remarks.

2. Study Area and Data Sources

2.1. Study Area. This article focuses on the areas of the Beijing-Tianjin-Hebei region that called Capital Circle in Northeast China—from the Taihang Mountains in the west to the Zhangbei Plateau in the north, the North China Plain in the south, and the Bohai Sea in the east. Figure 1 shows geographical position, topography, and gauges of the study area. The overall topography is high elevation in the northwest and low in the southeast [43]. The Beijing-Tianjin-Hebei region is situated within a warm-temperate monsoon climate, with dry springs and wet summers.

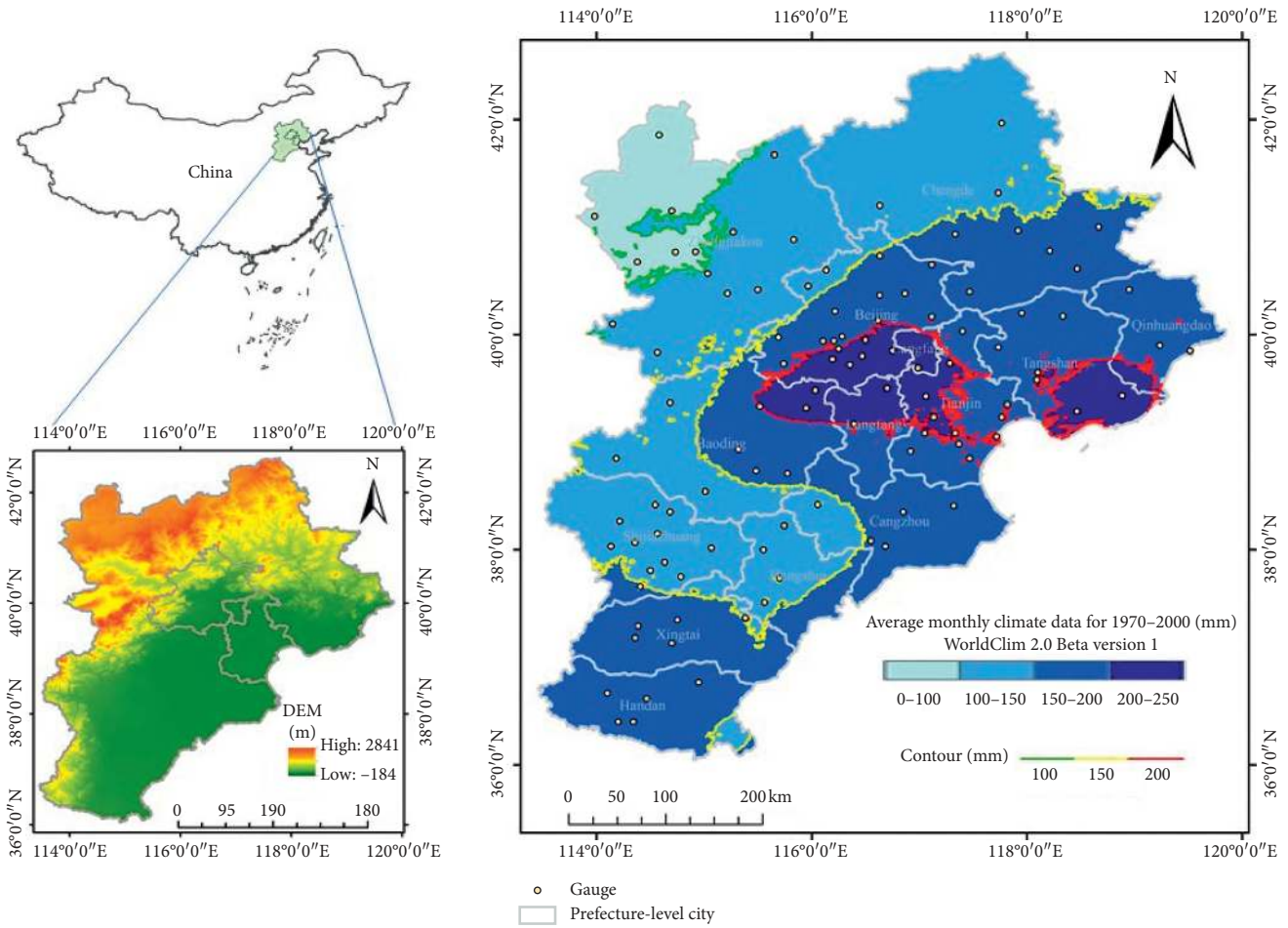

Figure 1: Geographical position, topography, and gauges of the study area.

2.2. GPM Products. Global Precipitation Measurement (GPM) is a new generation of satellite precipitation products. Its purpose is to develop the next generation of a space measurement system which can realize frequent and accurate global rainfall measurements [4]. Based on the success of TRMM, GPM focuses on deploying a "core" satellite, under joint development by NASA and the Japan Aerospace Exploration Agency (JAXA) [4]. Launched in February 2014, the Core Observatory combines advanced microwave detection techniques and data correction algorithms to provide more options for studying precipitation. It carries the first space-borne Ku-/Ka-band dual-frequency precipitation radar (DPR) and a multichannel GPM microwave imager (GMI) [4, 44]. The DPR instrument (Ku-band at 13.6 GHz and Ka-band at 35.5 GHz) provides three-dimensional measurements of precipitation structure which are more sensitive to rates of light rain and snowfall than the TRMM precipitation radar [44]. The GMI instrument (frequency from 10 GHz to 183 GHz) is a multichannel, conical-scanning, microwave radiometer, with the aim of measuring precipitation features such as intensity and type [13, 45]. Compared with TRMM which focuses on the observation of precipitation in the tropical and subtropical regions, GPM can capture low precipitation ($<0.5\ \mathrm{mm{\cdot}h^{-1}}$) and solid-state precipitation more accurately, extending measurements to ±68° latitude [4]. The GPM also extends the TRMM sensor load, significantly improving its precipitation observation capability. Its high-resolution precipitation products can reach 0.1° latitude/longitude spatial resolution and half-hourly temporal resolution.

IMERG is a level-3 GPM product and uses the algorithm Day-1 U.S. multi-satellite precipitation estimation which relies on three existing algorithms, namely, TMPA, CMORPH, and PERSIANN [46]. The algorithm aims at intercalibrating and merging "all" satellite microwave precipitation estimators, along with microwave-calibrated infrared (IR) satellite estimates, precipitation gauge analyses, and potentially other precipitation estimators. To obtain rainfall estimates for this study, firstly, all input datasets were processed using the Goddard profiling algorithm 2014 (GPROF2014) and IR rainfall estimates. Then, the rainfall estimates were recalibrated by the Climate Prediction Centre's (CPC) Morphing-Kalman Filter (CMORPHKF) using the Lagrangian time interpolation technique and the PERSIANN-Cloud Classification System (PERSIANN-CCS) to ensure products had 0.1° spatial and 30 min temporal resolutions. Finally, to improve the accuracy of the product, monthly Global Precipitation Climatology Center (GPCC) products were utilized to correct the bias.

These three latency periods, known as "early," "late," and "final," were delayed by about 6 hours, 18 hours, and 4 months, respectively, between the collection of observations and the generation of data products. The GPM (IMERG) final run version 4 product was used, which is the post-real-time research product in the IMERG suite [47].

The "final" IMERG has three kinds of datasets (Table 1): half-hourly scale data (hereafter called GPM-HH), daily scale data (hereafter called GPM-D), and monthly scale data (hereafter called GPM-M). These datasets are useful for long-time series analysis of precipitation events and for disaster risk. Therefore, in this paper, we evaluated the applicability of these three kinds of data in the Beijing-Tianjin-Hebei region. And, we corrected GPM-M and GPM-D products using Cumulative Distribution Function (CDF) model. The IMERG products were downloaded from the PMM website (http://pmm.nasa.gov/data-access/downloads/gpm).

2.3. Gauge Data. We screened the national meteorological stations in the Beijing-Tianjin-Hebei region. Some gauges with missing data were deleted, until 107 national meteorological stations were finally selected. Based on the site precipitation data, the adaptability of GPM products to Beijing, Tianjin, and Hebei at different timescales was evaluated (Figure 1). The dataset time series used was the monthly average precipitation from March 2014 to 2016; and the daily and hourly precipitation from January to December 2016. By obtaining the average monthly precipitation at each gauge, GPM-M products were evaluated. The period of participation in the evaluation was from March 2014 to December 2016. The precipitation was greatest in July–September, making verification more reliable during that time. Therefore, the daily and hourly precipitation data from 1 July to 30 September 2016 were selected for evaluation of GPM-D products and GPM-HH products. Finally, the monthly and daily precipitation data were used to correct GPM-M and GPM-D products using CDF model.

3. Methodology

3.1. Preprocess of GPM Products. The data in this article are referred to in World Time. GPM IMERG products are raster data. Table 1 illustrates the grid unit of the GPM-HH products in mm/h. Therefore, the hourly accumulation of 2 half-hourly precipitations was then multiplied by a factor of 0.5. These three types of data indicated the precipitation rate and therefore needed to be converted into actual rainfall in millimetres. The formulas are as follows:

$$\begin{aligned} y_{\mathbf{HH}} &= P \times 0.1 \times 0.5, \\ y_{\mathbf{D}} &= P \times 0.1 \times 24, \\ y_{\mathbf{M}} &= P \times 0.001 \times 24 \times N_{\mathbf{D}}, \end{aligned} \tag{1}$$

where $y_{\mathbf{HH}}$ is the rainfall of GPM-HH products; $y_{\mathbf{D}}$ is the rainfall of GPM-D products; $y_{\mathbf{M}}$ is the rainfall of GPM-M products; P is the GPM image grid value; and $N_{\mathbf{D}}$ is the number of days at different months.

3.2. Applicability Evaluation Indices. GPM products at different timescales were compared and analysed according to the grid point values of the corresponding meteorological stations and satellite precipitation data [25]. The quantitative and qualitative correlations between satellite rainfall and ground-based weather station rainfall data were evaluated using two kinds of quantitative indexes (mean) and correlation coefficients (CC). The mean was used to assess the accuracy of satellite precipitation products for rainfall measurements. The average showed the trend of satellite precipitation data in the region; and CC indicated the linear correlation between satellite rainfall data and ground-based weather station rainfall data. The precision evaluation of precipitation products of different magnitudes used Nash-Sutcliffe (NSE with a range of ∞ to 1) and normalized root mean square error (NRMSE) as indices [48]. The higher the NSE value, the closer the GPM value was to the gauged value and the better the simulation effect [49]. The ability to detect rainfall events from satellite rainfall data can be assessed comprehensively in three categories: False Alarm Ratio (FAR), Underreporting Rate (UR), and CSI. The lower the UR, the smaller the false negatives; the lower the FAR, the smaller the empty forecast. In fact, CSI is a more balanced score [22]. RMSE and BIAS are used to evaluate the accuracy of the modified GPM-M products. The root mean square error (RMSE) is used to assess the overall level of error and accurately reflect the accuracy of satellite precipitation products. When the Relative Bias (BIAS) is greater than 0, it shows that the estimated value of satellite is less than the measured value. The closer the BIAS is to 0, the better the agreement between the satellite detection effect and the measured value [49].

3.3. CDF Model. The gamma distribution has strong adaptability and can be fitted to many positive observation datasets. Precipitation distributions are usually skewed and many studies have shown that the gamma distribution is the best model for fitting to precipitation data [38–40]. The gamma distribution, denoted as Γ (α, β), had a probability density function:

$$f(x) = \begin{cases} \dfrac{1}{\beta^{\alpha}\Gamma(\alpha)} x^{\alpha-1} e^{-x/\beta}, & x > 0, \\ 0, & x = 0, \end{cases} \tag{2}$$

$$\Gamma(\alpha) = \int_0^{\infty} x^{\alpha-1} e^{-x}\, dx,$$

Here, x is the amount of precipitation in mm. Maximum likelihood estimation is used to determine the shape parameter α and the scale parameter β of each gamma distribution.

Table 1: GPM final IMERG products summary.

GPM products (latency)	Research contents	Abbreviation	Resolution	Dates	Precipitation units in GIS file
Final IMERG (4 months)	Adaptability evaluation	GPM-HH	0.1°–30 minutes	2016.07–2016.09	0.1 mm/h
		GPM-D	0.1°–1 day	2016.07–2016.09	0.1 mm/h
		GPM-M	0.1°–1 monthly	2014.03–2016.12	0.001 mm/h
	Data correction	GPM-D	0.1°–1 day	2016.07–2016.09	0.1 mm/h
		GPM-M	0.1°–1 monthly	2014.03–2016.12	0.001 mm/h

$$A = \ln\left(\frac{1}{n}\sum_{i=1}^{n} x_i\right) - \frac{1}{n}\sum_{i=1}^{n} \ln x_i,$$

$$\alpha = \frac{1 + \sqrt{1 + 4A/3}}{4A}, \tag{3}$$

$$\beta = \frac{\sum_{i=1}^{n} x_i}{n\alpha},$$

Here, A is the precipitation interval, x_i is the amount of precipitation in the sample, and n is the total number of samples. So, the CDF for precipitation over a given timescale can be expressed as follows:

$$f(x;\alpha,\beta) = \int_0^x f(t)\,dt. \tag{4}$$

The CDFs can be used to model precipitation data measured by both meteorological stations and the GPM satellite. The CDF curve fitted to the GPM data is corrected using the CDF curve for ground-measured precipitation. Since the amount of precipitation in the CDF model cannot be 0, it needs to be treated separately.

Assume that the monthly precipitation recorded by ground gauges is X_{Gauge}, the corresponding GPM precipitation is X_{GPM}, and the corrected precipitation is X'_{GPM}. Then, the specific process is shown in Figure 2.

(a) As shown in Figure 3, data from 107 sites are randomly divided into (1) 75 sites used for construction of the CDF model (training dataset); and (2) 32 sites for model accuracy verification (validation dataset).

(b) When $X_{\text{Gauge}} = 0$, let $X_{\text{GPM}} = 0$ to reduce the GPM satellite's empty reporting rate.

(c) When $X_{\text{Gauge}} > 0$, the CDF curves of the different precipitation ranges are established by using the meteorological station data for the study area, as $\text{CDF}_{\text{Gauge}}$. The corresponding CDF curves of GPM precipitation are recorded as CDF_{GPM}. Using $\text{CDF}_{\text{Gauge}}$ to correct CDF_{GPM}, we obtain the revised GPM precipitation of different precipitation ranges, X'_{GPM}. This can be expressed as follows:

$$X'_{\text{GPM}} = \text{CDF}_{\text{gauge}}^{-1}\left(\text{CDF}_{\text{GPM}}\left(X_{\text{GPM}}\right)\right). \tag{5}$$

(d) Use the validation dataset to verify the accuracy of the model.

(e) The CDF correction model is applied to the whole research area to achieve revised GPM-D and GPM-M data for the Beijing-Tianjin-Hebei region.

4. Results and Discussion

4.1. Adaptability Evaluation of GPM Products

4.1.1. Results of Adaptability Index. Based on the statistical metrics (Table 2), we evaluated GPM precipitation products based on the observation data of 107 ground meteorological stations. Table 3 shows that the correlation between GPM-HH products and the precipitation data of the gauges was lower, reaching only 0.38. The correlation between GPM-D products and the precipitation data of gauges was higher at 0.75. Compared with GPM-HH and GPM-D products, GPM-M products had strong correlation at 0.90. As the timescale increased, NSE showed a weaker trend while that of NRMSE tended to be stronger. The closer NSE was to 1, the closer were the GPM products and gauged values. The lower the NRMSE value, the smaller the error. Therefore, the GPM-M products show the smallest error and greatest accuracy. The GPM-HH products had the lowest accuracy. There may have been spatial heterogeneity, with great uncertainty [15]. Compared with half-hourly scale products, monthly and daily scale products showed smoother extreme values and lower errors relative to gauge measurements. The ability to detect precipitation events was analysed using FAR, UR, and CSI, with CSI having a more balanced score. As shown in Table 3, the UR, FAR, and CSI at the daily scale were 0.38, 0.20, and 0.53, respectively, better than those of the GPM-HH products. GPM-M products had the highest CSI and best detection ability for precipitation events. According to the trend shown in Table 3, the ability of the tested products to detect precipitation events, in order from high to low, were GPM-M, GPM-D, and GPM-HH.

4.1.2. Spatial Distribution of GPM-M's Adaptability. Based on Tyson polygons, the Beijing-Tianjin-Hebei region was divided into 107 polygons dictated by the locations of the 107 weather stations. Each polygon represented the largest influence range to obtain the spatial distribution of statistical indicators at different timescales and seasons. Figure 4 shows that satellite precipitation products at the monthly scale (GPM-M) were a good reflection of the precipitation events in the Beijing-Tianjin-Hebei region. Most of the region correlation coefficients were greater than 0.9. Meanwhile, GPM-M products had a higher NSE value and a lower NRMSE value with higher accuracy. GPM-M products also had the strongest detection ability for precipitation events. According to the spatial distribution of index, the GPM satellites were poorly represented in precipitation events in the marginal areas of the northwest and southeast of the Beijing-Tianjin-Hebei region. The regions

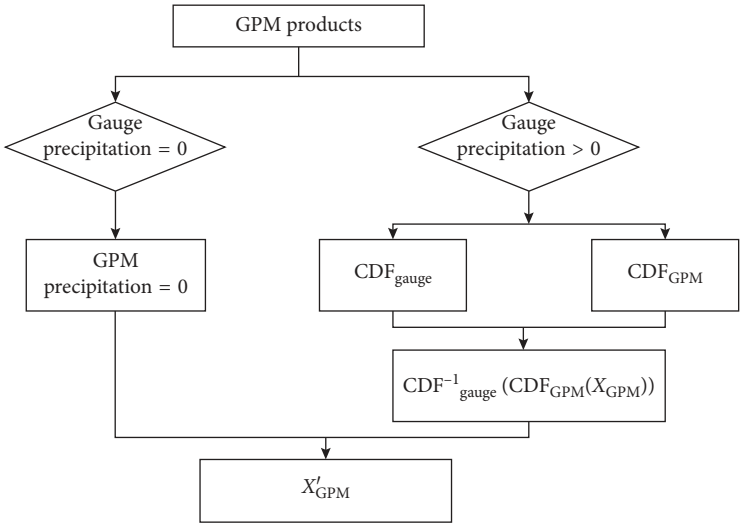

Figure 2: Flowchart of the CDF model for precipitation correction.

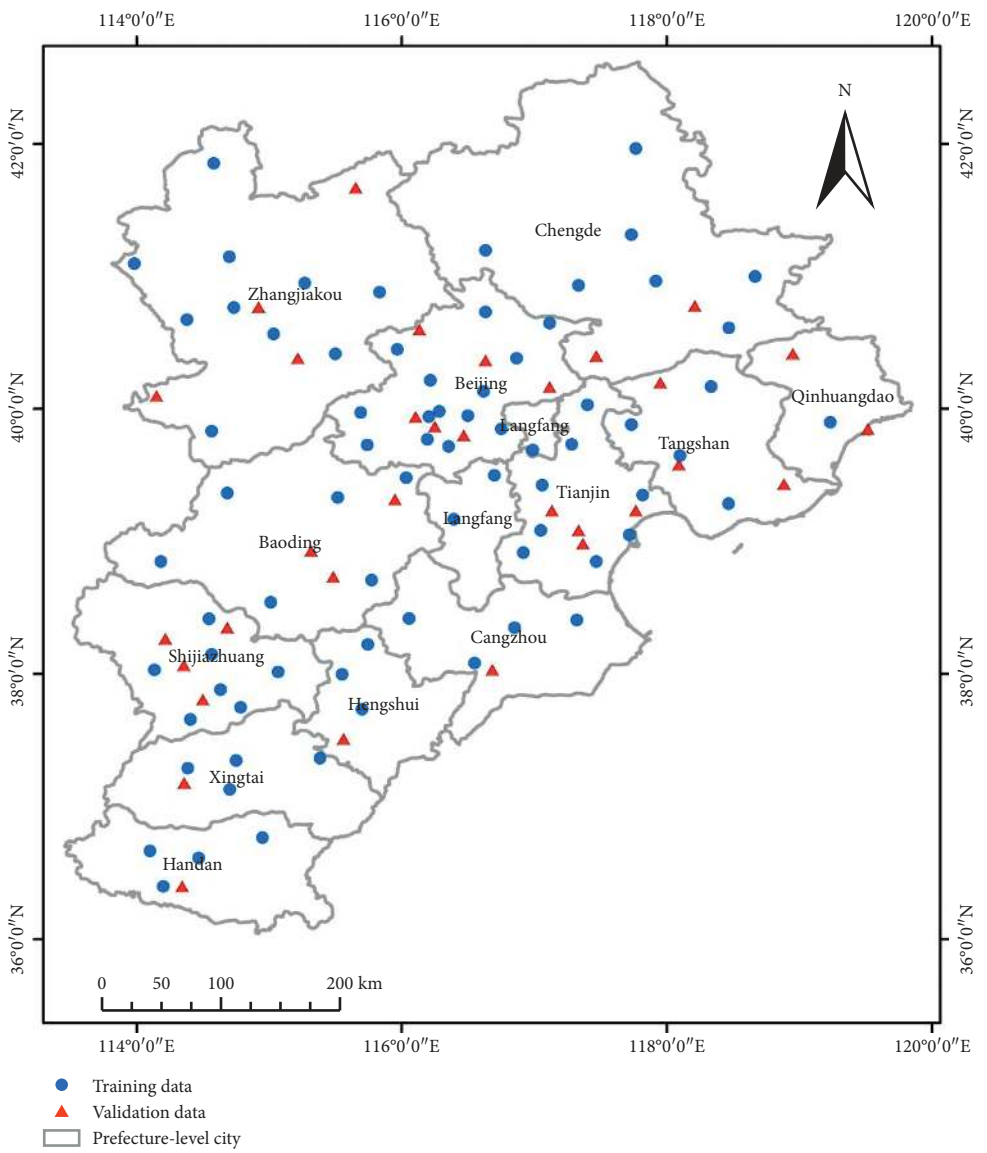

Figure 3: Distribution of training and validation data sources in the Beijing-Tianjin-Hebei region, China.

Table 2: List of the statistical metrics used in the evaluation.

Statistic metrics	Equation	Optimum value
Mean (M)	$M_x = 1/N\sum_{n=1}^{n} x_n$; $M_y = 1/N\sum_{n=1}^{N} y_n$	NA
Correlation coefficient (CC)	$\mathrm{CC} = \mathrm{Cov}(x_n - y_n)/\delta_x\delta_y$	1
NRMSE	$\mathrm{NRMSE} = (\sqrt{1/N\sum_{n=1}^{N}(x_n - y_n)})/(1/N\sum_{n=1}^{N} y_n)$	0
RMSE	$\mathrm{RMSE} = \sqrt{\sum_{n=1}^{N}(x_n - y_n)^2/N}$	0
BIAS	$\mathrm{BIAS} = (\sum_{n=1}^{N}(y_n - x_n))/(\sum_{n=1}^{N} y_n) \times 100\%$	0
NSE	$\mathrm{NSE} = 1 - (\sum_{n=1}^{N}(x_n - y_n)^2)/(\sum_{n=1}^{N}(y_n - \overline{y_n})^2)$	1
Underreporting rate (UR)	$\mathrm{UR} = n_{01}/n_{11} + n_{01}$	0
False alarm ratio (FAR)	$\mathrm{FAR} = n_{10}/n_{11} + n_{10}$	0
Critical success index (CSI)	$\mathrm{CSI} = n_{11}/n_{11} + n_{01} + n_{10}$	1

Note: n represents number of samples; x_n represents the satellite precipitation estimate; y_n represents the gauge observed precipitation; Cov() represents the covariance; δ_y represents standard deviations of gauge precipitation; δ_x represents standard deviations of satellite precipitation; n_{11} represents the precipitation observed by the gauge and satellite simultaneously; n_{01} represents the precipitation observed by the gauge but not observed by the satellite; n_{10} is contrary to n_{01}; and n_{00} represents the precipitation observed neither by the gauge nor the satellite.

Table 3: Adaptability index at different timescales (CC, NRMSE, NSE, UR, FAR, and CSI).

Statistical indicators	Consistency	Precision		Detection ability		
	CC	NRMSE	NSE	UR	FAR	CSI
GPM-HH	0.38	9.78	−0.3	0.46	0.58	0.31
GPM-D	0.75	2.87	0.53	0.38	0.2	0.53
GPM-M	0.90	0.58	0.8	0	0.06	0.94

coinciding with better satellite performance were mostly in the plains. The southeast of the Beijing-Tianjin-Hebei region is located on the coastline of the Bohai Sea. GPM satellites perform poorly in complex calibration systems that distinguish between rain and no rain [13]. With higher precipitation, the error of GPM products increases relatively, resulting in reduced data accuracy. Due to physical errors, it is very difficult for GPM sensors to detect deep convection caused by unstable air mass [13]. The areas in the northwest (mountainous) and southeast regions were unable to accurately detect precipitation events as they were not conducive to the transport of water vapor, so had less precipitation. GPM satellites had difficulties detecting microprecipitation. The contour map of precipitation was drawn according to the average monthly precipitation in July from 1970 to 2000, shown in Figure 1, and the areas of Beijing, Tianjin, and Hebei were divided by different rainfall intensities: 0–100 mm, 100–150 mm, 150–200 mm, and 200–250 mm. According to the correlation between GPM products and meteorological stations in different precipitation intensity areas, it was found that the correlation coefficient was low at 0–100 mm, mostly high between 150 and 200 mm, and higher areas with 200–250 mm were less. It could be seen that with greater precipitation intensity, the trend of the correlation between GPM and gauges increased first and then decreased slightly. This may have been due to the limitations in GPM for detecting microprecipitation, resulting in the lowest correlation in areas with relatively low precipitation. For higher rainfall areas, the GPM was prone to large deviation, with a slight decrease in precipitation of high-value area correlation. The comparison of GPM product accuracy for different precipitation intensity areas found that GPM-M products had the highest accuracy and performance in the region of 100–200 mm precipitation intensity. For different rainfall intensities, GPM products at different timescales had different performance capabilities (Figure 4). The GPM-M products had the weaker ability to detect precipitation in areas near the 150 mm contour.

4.1.3. Temporal Distribution of GPM-M's Adaptability. The amount of precipitation varies significantly throughout the seasons. Therefore, based on the monthly GPM products (GPM-M), the satellite data and gauge data of the 107 sites in the study area were classified according to the season (spring: March-May; summer: June-August; autumn: September-November; and winter: December-February); therefore, quarterly precipitation data were captured. Based on the correlation coefficients of the different seasons (Figure 5), the correlation coefficient of spring and winter was slightly higher than that of summer and autumn. However, the performance of GPM products at autumn and summer is better than that of spring and winter. In spring and winter, the research area is dry and cold, mainly showing small amounts of precipitation and snowfall, which is a great disturbance to the detection of precipitation by GPM products. The precipitation in summer and autumn is higher than that in spring and winter; that is, the performance of GPM products in wet season is better than that in the dry season. Figure 6 shows the quarterly average rainfall at all stations from the GPM products and gauges from March 2014 to December 2016. Based on the figure, we can see the rainfall distribution of satellite data is in good agreement with the data of ground meteorological stations, which can well reflect the rainfall in each season. However, there are some deviations in the specific quantities and GPM estimates are generally overvalued.

4.2. GPM Products Correction and Accuracy Verification

4.2.1. Data Correction Based on CDF Model. We used precipitation data from 75 national meteorological stations and the GPM products to build CDF curves for correcting

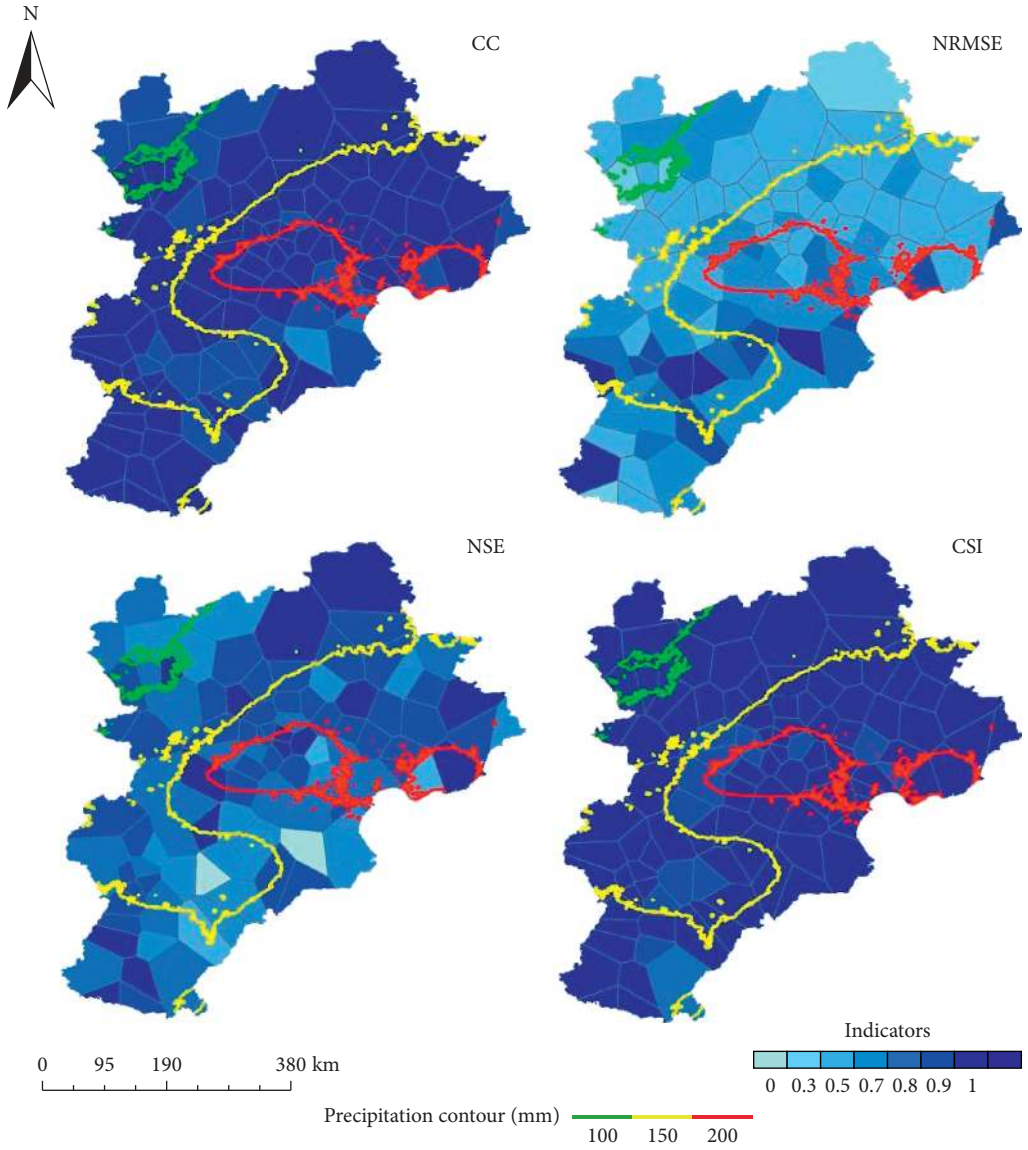

Figure 4: Spatial distribution of CC, NRMSE, NSE, and CSI based on GPM-M products.

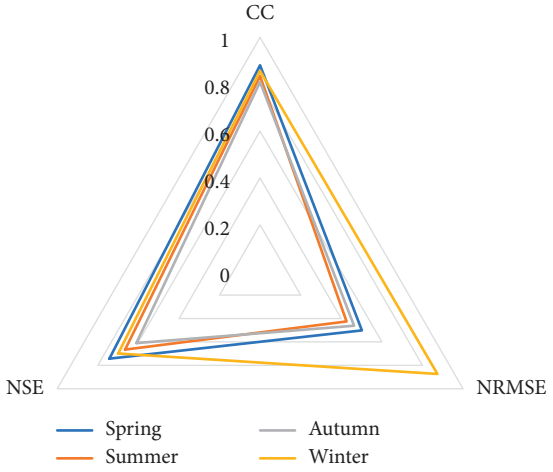

Figure 5: Numerical values of CC, NRMSE, and NSE at the seasonal scale.

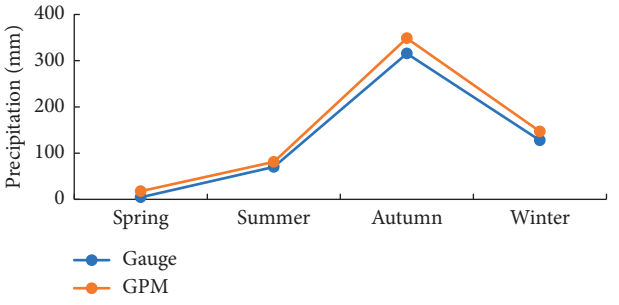

Figure 6: The average monthly rainfall of all gauges and GPM monthly data.

the GPM data. Table 4 shows the shape parameter α and scale parameter β for the two CDF models.

Figure 7(a) is a graph based on the CDF models (day), in which the green line is the CDF curve of the gauge data, the

Table 4: CDF model shape parameter α and scale parameter β.

	Gauge		GPM	
	α	β	α	β
CDF model (day)	0.6469	75.2344	0.8139	66.8997
CDF model (month)	0.5462	34.4265	0.7976	26.814

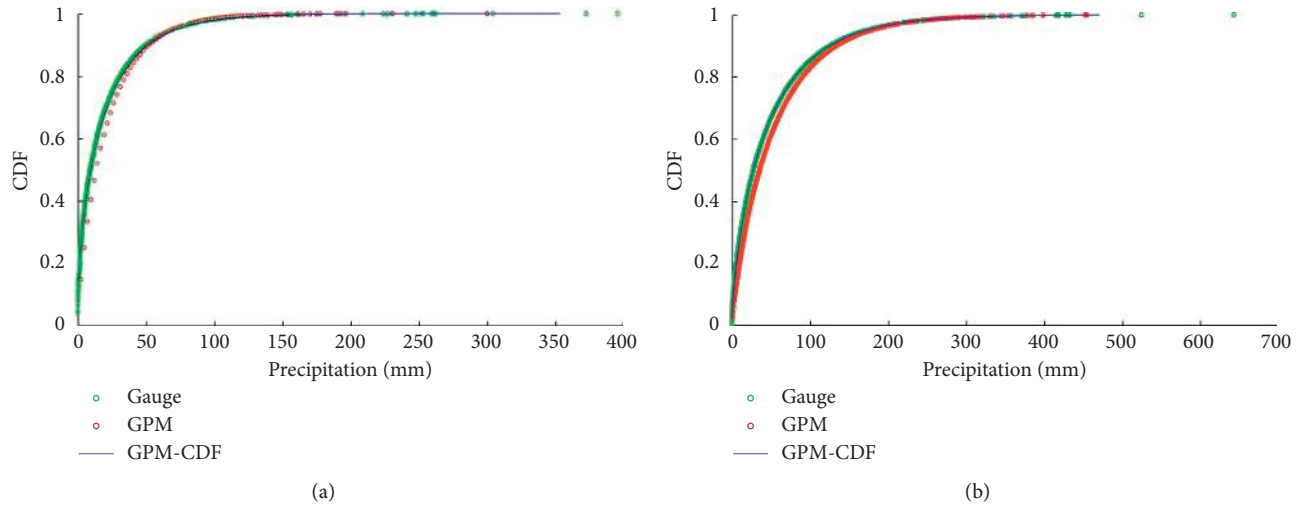

Figure 7: CDF curves for gauge, GPM, and GPM-CDF datasets. (a) Day; (b) month.

red line is the CDF curve of GPM-D precipitation training data, and the blue line is the CDF curve of CDF precipitation validation data through the CDF model. Figure 7(b) is a graph based on the CDF models (month), in which the red line is the CDF curve of GPM-M precipitation training data. After calibration, the CDF curve is more and more consistent with the CDF curve of the gauge data, indicating the effectiveness of the modified model. Table 5 shows the precision of the CDF model. The correlation of the CDF model was slightly lower than the correlation of the GPM original precipitation product. However, the RMSE of the CDF model was less than that of the original data, while the precision increased. The BIAS of the CDF model was close to 0, indicating that the agreement between the satellite and ground-measured data was good. Because the BIAS was less than 0, it indicates that the GPM data were underestimated. Therefore, the CDF model is suitable for GPM-M and GPM-D data correction in the study area.

4.2.2. Accuracy Verification of the CDF Model. To further quantify the accuracy of the CDF correction model, monthly precipitation data from 32 national data stations were used to verify the model (verification dataset). It can be seen from Table 6 that the accuracy of the GPM-D and GPM-M data was improved after correction although it was overestimated. Figure 8 shows the CDF correction results. The abscissa represents the month and the ordinate represents the average monthly precipitation. Figure 8(a) shows that the calibrated result is closer to the real value. When the average monthly precipitation is larger, the correction effect is better. At the same time, when the GPM precipitation is greater than the gauge precipitation, GPM-M products can be better corrected. When the GPM precipitation is less than the site precipitation, the corrected result often deviates more from the real value (Figure 8, red box). The main reason is that when the GPM precipitation is less than the site precipitation, the CDF curve of GPM precipitation is under the gauge CDF curve after trend fitting, which makes the corrected GPM value smaller than the gauge data. Figure 8(b) shows the results of the CDF model (day). After correction, the precipitation of GPM-D product is closer to the real value.

Table 5: Comparison of the CDF model results.

Statistical indicators	CC	RMSE	BIAS (%)
GPM-D	0.7500	12.3831	−7.58
CDF model (day)	0.7839	10.5738	4.53
GPM-M	0.9031	26.3928	12.31
CDF model (month)	0.9028	25.7803	0.12

Table 6: CDF model verification results.

Model validation	CC	RMSE	BIAS (%)
GPM-D	0.7569	12.9672	6.75
GPM_{CDF} (day)	0.7959	11.6452	4.76
GPM-M	0.9159	26.0057	0.56
GPM_{CDF}(month)	0.9167	25.3933	0.92

Since the CDF model is better than the original data, we further discuss the correction effect of the correction model in each precipitation interval. Because the daily precipitation range is small, GPM-M data are selected for discussion. As shown in Table 7, correction worked best in the ranges of 0–100 mm and >200 mm. Because of the presence of trace

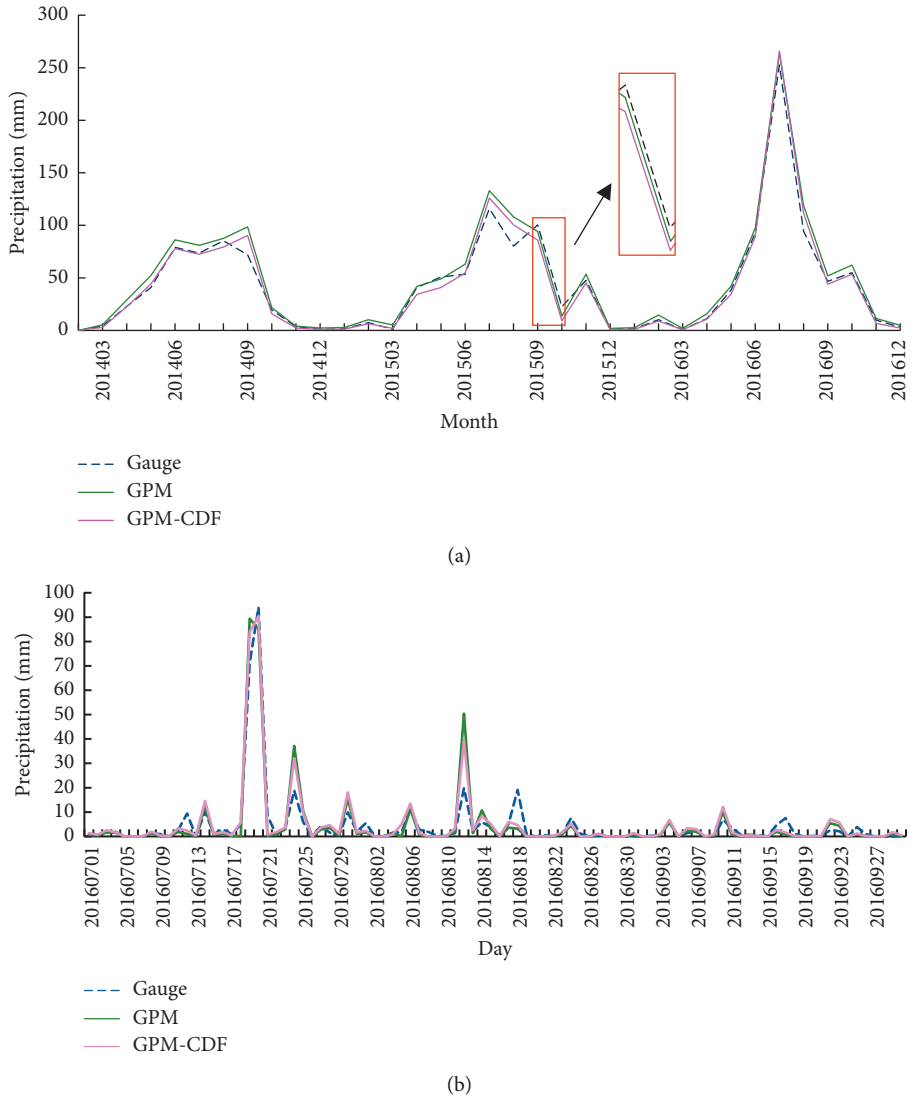

Figure 8: The results of the CDF model. (a) Month and (b) day.

precipitation in the 0–100 mm interval, the accuracy of GPM will be affected. High precipitation (>200 mm) results in larger GPM precipitation errors. The CDF-segmented model can effectively correct the errors caused by trace precipitation and extreme precipitation. Among them, the accuracy of corrected GPM-M data was highest in the 0–100 mm interval, but the data were underestimated. The corrected GPM-M products in the >100 mm range were overestimated.

4.3. Analysis of Temporal and Spatial Distribution Characteristics of Precipitation Based on Corrected GPM-M Products

4.3.1. Interannual Variation of Precipitation. We used GPM-M data modified by the CDF model to analyse the spatial and temporal distributions of precipitation in the study area. This paper synthesized corrected GPM-M data and annual data to obtain a mean annual precipitation map (Figure 9). As can be seen from Figure 10, the highest annual precipitation was concentrated in the northeastern area, where it reached 820 mm. The lowest annual precipitation was concentrated in the northwest. From the northwest to the southeast, the precipitation decreased gradually and showed a clear banded distribution.

4.3.2. Precipitation Changes during the Year. Based on the CDF-corrected GPM-M data, the mean monthly precipitation distribution in the area was calculated (Figure 10). The monthly distribution was approximately the same as the annual one; however, in July, precipitation in the sub-high-value areas of annual precipitation was the highest and had a banded distribution. From November to March of the following year, precipitation in this area was almost <50 mm and precipitation was scarce. From April to June, the monthly precipitation gradually increased, and the high precipitation still occurred in the northeast. Precipitation mostly occurred in July and August, with a maximum of

Table 7: CDF model verification results according to precipitation range.

		0–100 mm		100–150 mm		150–200 mm		>200 mm	
	Indicators	GPM	GPM_{CDF}	GPM	GPM_{CDF}	GPM	GPM_{CDF}	GPM	GPM_{CDF}
Training dataset	CC	0.8505	0.8359	0.298	0.2976	0.3146	0.3135	0.597	0.5993
	RMSE	21.1972	19.3445	34.9012	37.677	46.3524	50.6796	77.0531	79.635
	BIAS (%)	26.56	7.3	2.79	9.06	8.23	11.68	8.45	8.08
Validation dataset	CC	0.8741	0.8622	0.2196	0.2173	0.4686	0.4686	0.658	0.6582
	RMSE	19.7058	17.5907	36.7289	38.3842	52.6878	58.3426	72.5152	74.9895
	BIAS (%)	26.6	7.4	2.01	4.21	16.38	20.06	10.7	10.24

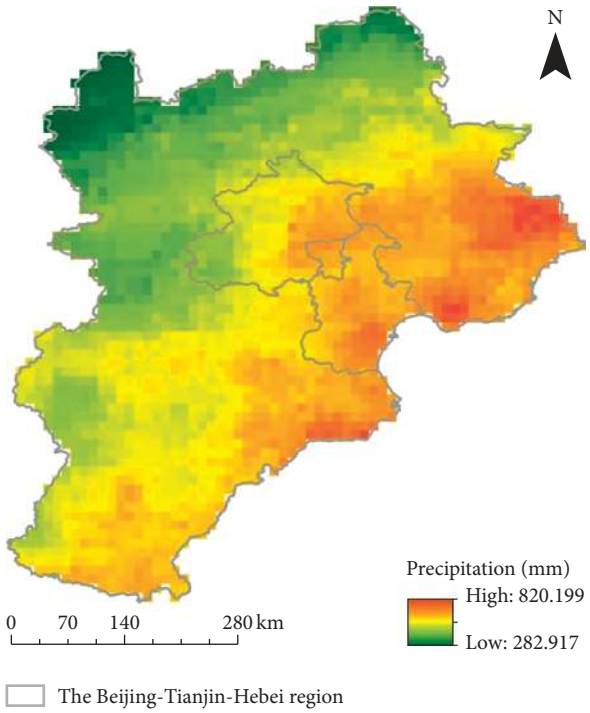

Figure 9: Mean annual precipitation based on modified GPM-M data (CDF model).

250 mm. Meanwhile, precipitation in September and October gradually decreased. In summary, the distribution of precipitation in the area shows clear heterogeneity in different months, and the difference in precipitation in different areas is clearer.

5. Conclusion

This study conducted a comparative analysis of the precipitation data of GPM products (Final Run) and the precipitation data of 107 gauges in the Beijing–Tianjin–Hebei region. To begin with, we analysed the applicability and spatial characteristics of GPM products in different timescales. Next, we used the CDF model to correct GPM-M products. Finally, we analysed the temporal and spatial distribution characteristics of precipitation based on modified GPM-M products and reached the following conclusions:

(1) The GPM-M products have strong applicability and accurately reflected the precipitation events in the Beijing-Tianjin-Hebei region. Based on the comparison of the monthly mean rainfall, the 12-month rainfall distribution of satellite data was in good agreement with the data of ground meteorological stations, which well reflected the rainfall for each month. However, these are still overrated. The performance of GPM products in summer and autumn was better than in winter and spring, and the performance of GPM products in the wet season at a monthly scale was better than in the dry season. Therefore, GPM-M products could be used as the basic data of a hydrological model. However, GPM products have poor detection capability in areas with extremely undulating terrain, such as mountainous areas. Also, the spatial resolution of rainfall data is still relatively coarse, potentially leading to error.

(2) With an increase in precipitation intensity, the correlation between GPM products and sites had a trend of first increasing and then decreasing slightly, highlighting that GPM products may have uncertainty for extreme precipitation and trace precipitation.

(3) The accuracy of the CDF-corrected GPM data is better than that of the original GPM-D and GPM-M product. The GPM product will be more accurately corrected when the GPM-estimated precipitation is greater than the gauge-measured precipitation. When GPM precipitation is less than the gauge-measured precipitation, the corrected results tend to deviate more from the real values. The GPM-M data range of 0–100 mm can be corrected best. Based on the CDF-corrected GPM-M data, the spatial distribution of mean annual precipitation decreases from northwest to southeast across the study area, with a roughly banded distribution. The distribution of monthly precipitation is obviously uneven, but its trend is roughly the same as that of mean annual precipitation.

In general, GPM is a new generation of precipitation observation satellites with high spatial-temporal resolution. GPM-D products and GPM-M products have strong detection capability for rainfall events, and the accuracy of correction GPM products increase, which can provide data support for long-time series analysis in the Beijing-Tianjin-Hebei region. However, due to various factors such as elevation, topography, and longitudinal and latitudinal gradient, it is necessary to further improve the quality and spatial resolution of GPM to provide a more accurate

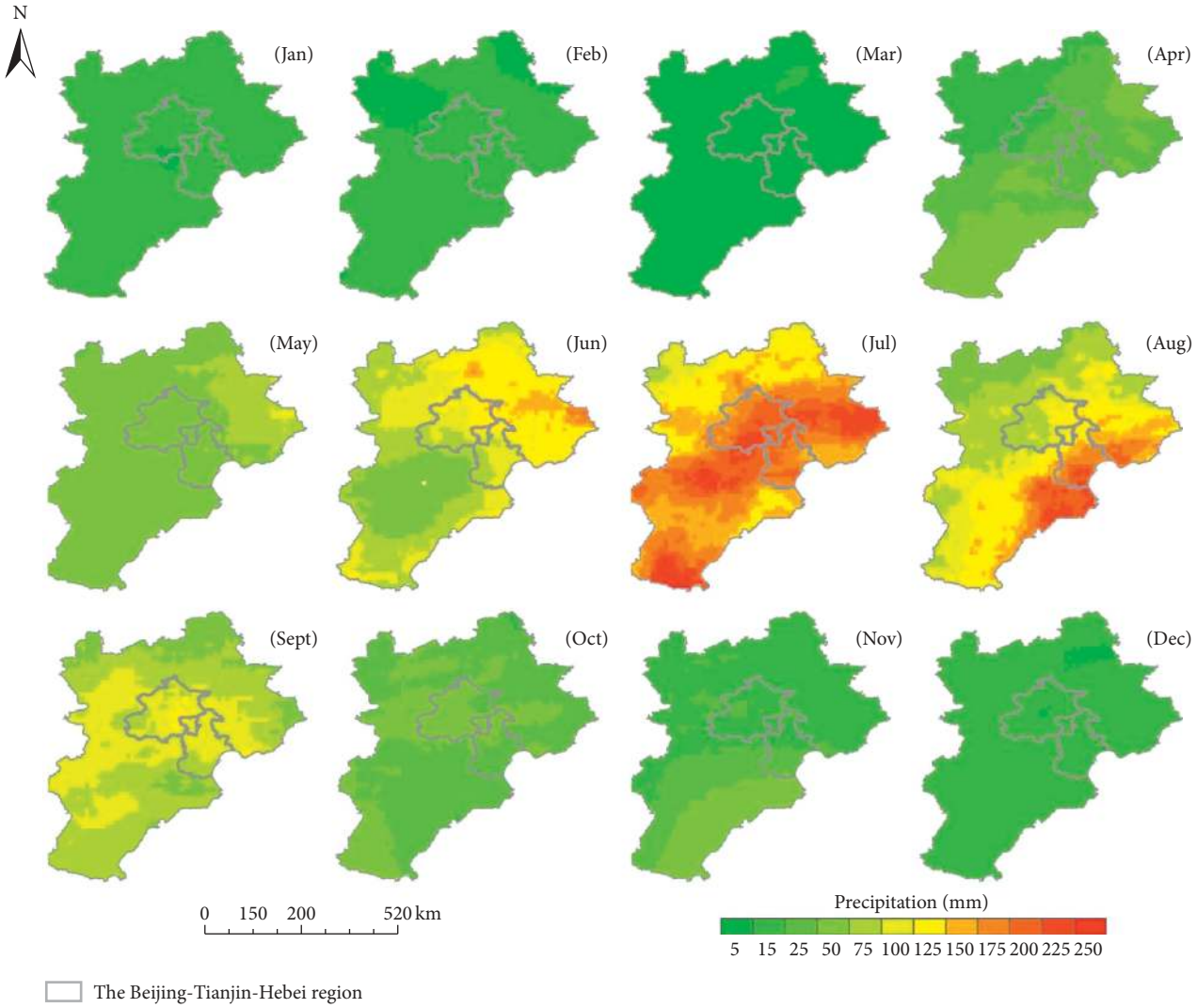

Figure 10: Spatial distribution of mean monthly precipitation in the study area.

estimation of future precipitation. It is of great practical significance to reveal the variations and regularity of precipitation and improve the ability of precipitation estimation for areas lacking data. In the study of global climate change, hydrological cycles, the ecological environment, and other scientific research, GPM should be of great value. If it can be applied to agricultural production and disaster prevention, as well as other fields involving disaster assessment and risk prediction, it will have tremendous socioeconomic benefits. Therefore, finding ways to improve the data spatial resolution in the study area will be the main content of our next study.

Data Availability

The data used to support the findings of this study are available from the corresponding author upon request.

Conflicts of Interest

The authors declare no conflicts of interest.

Acknowledgments

This paper was jointly supported by the National Key R&D Program of China (2017YFC0406006 and 2017YFC0406004) and Science Foundation of Beijing Municipal Education Commission (SQKM201710028013). The authors would like to thank the China Meteorological Administration for providing ground-based rainfall data. The GPM products were provided by the NASA Goddard Space Flight Centre's Precipitation Processing System (PPS).

References

[1] Y. Yang, J. Du, and L. Cheng, "Evaluation of accuracy and reliability of TRMM satellite precipitation data in Hunan Province," *Journal of Water Resources & Water Engineering*, vol. 27, no. 1, pp. 26–32, 2016.

[2] X. Liu, J. Zhao, H. Zhang, X. Guo, Z. Zhang, and Y. Fu, "Accuracy validation and application of TRMM precipitation data in Northeast China," *Journal of Natural Resources*, vol. 30, no. 6, pp. 1047–1056, 2015.

[3] T. Ji, H. Yang, R. Liu, T. He, and J. Wu, "Applicability analysis of the TRMM precipitation data in the Sichuan-Chongqing region," *Progress in Geography*, vol. 33, no. 10, pp. 1375–1386, 2014.

[4] G. J. Huffman, R. F. Adler, P. Arkin et al., "The global precipitation climatology project (GPCP) combined precipitation dataset," *Bulletin of the American Meteorological Society*, vol. 78, no. 1, pp. 5–20, 1997.

[5] Z. Yao, W. Li, H. Gao, Y. Zhu, B. Zhao, and Q. Zhang, "Remote sensing of flooding using TRMM the microwave imager," *Acta Meteorologica Sinica*, vol. 60, no. 2, pp. 243–249, 2002.

[6] H. Zeng and L. Li, "Accuracy validation of TRMM 3B43 data in Lancang river basin," *Acta Geographica Sinica*, vol. 66, no. 7, pp. 994–1004, 2011.

[7] X.-H. Li, Q. Zhang, and C.-Y. Xu, "Suitability of the TRMM satellite rainfalls in driving a distributed hydrological model for water balance computations in Xinjiang catchment, Poyang lake basin," *Journal of Hydrology*, vol. 426-427, pp. 28–38, 2012.

[8] Y. Yang, G. Cheng, J. Fan, J. Sun, and W. Li, "Accuracy validation of TRMM 3B42 data in Sichuan basin and the surrounding areas," *Journal of the Meteorological Sciences*, vol. 33, no. 5, pp. 526–535, 2013.

[9] G. Zhu, T. Pu, T. Zhang, H. Liu, X. Zhang, and F. Liang, "The accuracy of TRMM precipitation data in Hengduan mountainous region, China," *Scientia Geographica Sinica*, vol. 33, no. 9, 2013.

[10] N. Yang, K. Zhang, Y. Hong et al., "Evaluation of the TRMM multisatellite precipitation analysis and its applicability in supporting reservoir operation and water resources management in Hanjiang basin, China," *Journal of Hydrology*, vol. 549, pp. 313–325, 2017.

[11] E. Sharifi, R. Steinacker, and B. Saghafian, "Assessment of GPM-IMERG and other precipitation products against gauge data under different topographic and climatic conditions in Iran: preliminary results," *Remote Sensing*, vol. 8, 2016.

[12] S. Khodadoust Siuki, B. Saghafian, and S. Moazami, "Comprehensive evaluation of 3-hourly TRMM and half-hourly GPM-IMERG satellite precipitation products," *International Journal of Remote Sensing*, vol. 38, pp. 558–571, 2016.

[13] K. Kim, J. Park, J. Baik, and M. Choi, "Evaluation of topographical and seasonal feature using GPM IMERG and TRMM 3B42 over Far-East Asia," *Atmospheric Research*, vol. 187, pp. 95–105, 2017.

[14] D. Sahlu, E. I. Nikolopoulos, S. A. Moges, E. N. Anagnostou, and D. Hailu, "First evaluation of the day-1 IMERG over the upper blue Nile Basin," *Journal of Hydrometeorology*, vol. 17, pp. 2875–2882, 2016.

[15] Z. E. Asong, S. Razavi, H. S. Wheater, and J. S. Wong, "Evaluation of integrated multisatellite retrievals for GPM (IMERG) over southern Canada against ground precipitation observations: a preliminary assessment," *Journal of Hydrometeorology*, vol. 18, pp. 1033–1050, 2017.

[16] S. Prakash, A. K. Mitra, D. S. Pai, A. AghaKouchak, H. Norouzi, and D. S. Pai, "From TRMM to GPM: how well can heavy rainfall be detected from space?," *Advances in Water Resources*, vol. 88, pp. 1–7, 2016.

[17] M. Tan and Z. Duan, "Assessment of GPM and TRMM precipitation products over Singapore," *Remote Sensing*, vol. 9, 720 pages, 2017.

[18] E. Sharifi, R. Steinacker, and B. Saghafian, "Hourly comparison of GPM-IMERG-final-run and IMERG-real-time (V-03) over a dense surface network in Northeastern Austria," *Geophysical Research Abstracts*, vol. 19, 2017.

[19] F. Satgé, A. Xavier, R. P. Zolá et al., ""Comparative assessments of the latest GPM mission's spatially enhanced satellite rainfall products over the main Bolivian watersheds," *Remote Sensing*, vol. 9, pp. 1–16, 2017.

[20] F. Alexander, A. Véliz, C. Leónidas, T. Ramos, and L. Waldo Sven, "Assessment of tropical rainfall measuring mission (TRMM) and global precipitation measurement (GPM) products in hydrological modeling of the Huancane river basin, Peru," *Scientia Agropecuaria*, vol. 9, no. 1, pp. 53–62, 2018.

[21] F. Chiaravalloti, L. Brocca, A. Procopio, C. Massari, and S. Gabriele, "Assessment of GPM and SM2RAIN-ASCAT rainfall products over complex terrain in southern Italy," *Atmospheric Research*, vol. 206, pp. 64–74, 2018.

[22] G. Tang, Y. Ma, D. Long, L. Zhong, and Y. Hong, "Evaluation of GPM Day-1 IMERG and TMPA Version-7 legacy products over Mainland China at multiple spatiotemporal scales," *Journal of Hydrology*, vol. 533, pp. 152–167, 2016.

[23] R. Xu, F. Tian, L. Yang, H. Hu, H. Lu, and A. Hou, "Ground validation of GPM IMERG and TRMM 3B42V7 rainfall products over southern Tibetan Plateau based on a high-density rain gauge network," *Journal of Geophysical Research: Atmospheres*, vol. 122, pp. 910–924, 2017.

[24] S. Ning, J. Wang, J. Jin, and H. Ishidaira, "Assessment of the latest GPM-era high-resolution satellite precipitation products by comparison with observation gauge data over the Chinese mainland," *Water*, vol. 8, pp. 8–11, 2016.

[25] X. Jin, H. Shao, C. Zhang, and Y. Yan, "The applicability evaluation of three satellite products in Tianshan Mountains," *Journal of Natural Resources*, vol. 31, no. 12, pp. 2074–2085, 2016.

[26] X. Tan, J. Wang, G. Liu, and Z. Zhu, "Study on extreme precipitation monitoring based on multi-satellite remote sensing products," *Geomatics World*, vol. 24, pp. 82–87, 2017.

[27] R. Wang, J. Chen, and X. Wang, "Comparison of IMERG level-3 and TMPA 3B42V7 in estimating typhoon-related heavy rain," *Water*, vol. 9, pp. 1–15, 2017.

[28] Z. Wang, R. Zhong, C. Lai, and J. Chen, "Evaluation of the GPM IMERG satellite-based precipitation products and the hydrological utility," *Atmospheric Research*, vol. 196, pp. 151–163, 2017.

[29] L. Li, W. Zhang, L. Yi, J. Liu, and H. Chen, "Accuracy evaluation and comparison of GPM and TRMM precipitation product over Mainland China," *Advances in Water Science*, vol. 29, no. 3, pp. 303–313, 2018.

[30] Z. Wei, G. Yue, J. Li, and T. Lv, "Comparison study on accuracies of precipitation data using GPM and TRMM product in Haihe river basin," *Bulletion of Soil and Water Conservation*, vol. 37, no. 2, pp. 171–176, 2017.

[31] Y. Tian, C. D. Peters-lidard, and J. B. Eylander, "Real-time bias reduction for satellite-based precipitation estimates," *Journal of Hydrometeorology*, vol. 11, no. 6, pp. 1275–1285, 2010.

[32] X. Zhang and Q. Tang, "Combining satellite precipitation and long-term ground observations for hydrological monitoring in China," *Journal of Geophysical Research: Atmospheres*, vol. 120, no. 12, pp. 6426–6443, 2015.

[33] A. AghaKouchak, N. Nasrollahi, and E. Habib, "Accounting for uncertainties of the TRMM satellite estimates," *Remote Sensing*, vol. 1, no. 3, pp. 606–619, 2009.

[34] M. Jehanzeb, M. Cheema, and W. G. M. Bastiaanssen, "Local calibration of remotely sensed rainfall from the TRMM satellite for different periods and spatial scales in the Indus

Basin," *International Journal of Remote Sensing*, vol. 33, no. 8, pp. 2603–2627, 2011.

[35] H. Guo, S. Chen, A. Bao et al., "Early assessment of integrated multi-satellite retrievals for global precipitation measurement over China," *Atmospheric Research*, vol. 176-177, pp. 121–133, 2016.

[36] X. Jin, H. Shao, Y. Qiu, and H. Du, "Correction method of TRMM satellite precipitation data in Tianshan Mountains," *Meteorological Monthly*, vol. 44, no. 7, pp. 882–891, 2018.

[37] W. Xiao and J. Xu, "Applied research of calibration method for SDSM model based on cumulative distribution function," *Acta Agricultures Jiangxi*, vol. 28, no. 1, pp. 74–78, 2016.

[38] Y. Ding, "Research of universality of Γ distribution model of precipitation," *Scinece Atmospherica Sinica*, vol. 18, no. 5, pp. 552–560, 1994.

[39] T. B. Mckee, N. J. Doesken, and J. Kleist, "The relationship of drought frequency and duration to time scales," in *Proceedings of the 8th Conference on Applied Climatology*, pp. 179–184, American Meteorological Society, Anaheim, CA, USA, January 1993.

[40] A. V. M. Ines and J. W. Hansen, "Bias correction of daily GCM rainfall for crop simulation studies," *Agricultural and Forest Meteorology*, vol. 138, pp. 44–53, 2006.

[41] J. Liu, "The temporal-spatial variation characteristics of precipitation in Beijing-Tianjin-Hebei during 1961-2012," *Climate Change Research Letters*, vol. 3, pp. 146–153, 2014.

[42] J. Wang, D. Jiang, and Y. Zhang, "Analysis on spatial and temporal variation of extreme climate events in North China," *Chinese Journal of Agrometeorology*, vol. 33, pp. 166–173, 2012.

[43] A. Zhang, S. Li, and X. Zhao, "Rainstorm risk assessment of Beijing-Tianjin-Hebei region based on TRMM data," *Journal of Natural Disasters*, vol. 26, pp. 160–168, 2017.

[44] A. Y. Hou, R. K. Kakar, S. Neeck et al., "The global precipitation measurement mission," *Bulletin of the American Meteorological Society*, vol. 95, pp. 701–722, 2014.

[45] G. Huffman, D. Bolvin, D. Braithwaite, K. Hsu, and R. Joyce, *Algorithm Theoretical Basis document (ATBD) NASA Global Precipitation Measurement (GPM) Integrated Multi-Satellite Retrievals for GPM (IMERG)*, NASA, Washington, DC, USA, 2013.

[46] G. J. Huffman, N. Gsfc, D. T. Bolvin, D. Braithwaite, K. Hsu, and R. Joyce, *Algorithm Theoretical Basis Document (ATBD) NASA Global Precipitation Measurement (GPM) Integrated Multi-SatellitE Retrievals for GPM (IMERG)*, NASA, Washington, DC, USA, 2014.

[47] G. Huffman, D. Bolvin, D. Braithwaite et al., "First results from the integrated multi-satellite retrievals for GPM (IMERG)," in *Proceedings of EGU General Assembly Conference*, Vienna, Austria, April 2015.

[48] Y. Liu, Y. Wu, Z. Feng, X. Huang, and D. Wang, "Evaluation of a variety of satellite retrieved precipitation products based on extreme rainfall in China," *Tropical Geography*, vol. 37, no. 3, pp. 417–433, 2017.

[49] X. Cai, S. Zou, Z. Lu, B. Xu, and A. Long, "Evaluation of TRMM monthly precipitation data over the inland river basins of Northwest China," *Journal of Lanzhou University*, vol. 49, no. 3, pp. 291–298, 2013.